Puerarin@Chitosan composite for infected bone repair through mimicking the bio-functions of antimicrobial peptides

Liping Ouyang [a,b], Baohui Chen [a], Xingdan Liu [a], Donghui Wang [a], Yang Li [d], Yun Liao [b], Kelvin W.K. Yeung [e], Xuanyong Liu [a,c,*]

[a] *State Key Laboratory of High Performance Ceramics and Superfine Microstructure, Shanghai Institute of Ceramics, Chinese Academy of Sciences, Shanghai, 200050, China*
[b] *Hongqiao International Institute of Medicine, Shanghai Jiao Tong University School of Medicine, Shanghai, 200336, China*
[c] *Cixi Center of Biomaterials Surface Engineering, Ningbo, 315300, China*
[d] *Department of Computational Biology for Individualised Medicine, Centre for Individualised Infection Medicine (CiiM) & TWINCORE, Joint Ventures Between the Helmholtz-Centre for Infection Research (HZI) and the Hannover Medical School (MHH), Hannover, Germany*
[e] *Shenzhen Key Laboratory for Innovative Technology in Orthopaedic Trauma, Guangdong Engineering Technology Research Center for Orthopaedic Trauma Repair, Department of Orthopaedics and Traumatology, The University of Hong Kong Shenzhen Hospital, Shenzhen, China*

ARTICLE INFO

ABSTRACT

It is important to eliminate lipopolysaccharide (LPS) along with killing bacteria in periprosthetic joint infection (PJI) therapy for promoting bone repair due to its effect to regulate macrophages response. Although natural antimicrobial peptides (AMPs) offer a good solution, the unknown toxicity, high cost and exogenetic immune response hamper their applications in clinic. In this work, we fabricated a nanowire-like composite material, named P@C, by combining chitosan and puerarin via solid-phase reaction, which can finely mimic the bio-functions of AMPs. Chitosan, serving as the bacteria membrane puncture agent, and puerarin, serving as the LPS target agent, synergistically destroy the bacterial membrane structure and inhibit its recovery, thus endowing P@C with good antibacterial property. In addition, P@C possesses good osteoimmunomodulation due to its ability of LPS elimination and macrophage differentiation modulation. The *in vivo* results show that P@C can inhibit the LPS induced bone destruction in the *Escherichia coli* infected rat. P@C exhibits superior bone regeneration in *Escherichia coli* infected rat due to the comprehensive functions of its superior antibacterial property, and its ability of LPS elimination and immunomodulation. P@C can well mimic the functions of AMPs, which provides a novel and effective method for treating the PJI in clinic.

1. Introduction

Periprosthetic joint infection (PJI) therapy requires implants possessing superior antibacterial and osteogenic effect to reduce the implant failure and the risk of patients' life after joint arthroplasty [1–4]. Herewith, traditional bone implant design pursues materials possessing superior antibacterial properties to address these problems [5–9]. During the past decades, many excellent antibacterial materials have been fabricated and applied in clinic. However, the post-orthopedic surgeries complications, such as septic shock, pyrogenic reaction, and blood clotting, often occur leading to an implant failure and even a life threat in patients [10–14]. These complications appear along with the rapid antibacterial therapy due to the explosive lipo-polysaccharides (LPS, also named endotoxin) release, resulting in overactive immune response. LPS is one of the major components of gram-negative bacteria outer membrane, which maintains bacteria structure and connects each bacterium to form bio-film [15]. Once the bacteria are sterilized, the dissociated LPS molecule could be recognized by Toll-Like receptor 4 (TLR4), thus mediating M1 macrophage activation [16]. M1 would subsequently release several inflammatory cytokines, such as interleukin (IL-1), tumor necrosis factor (TNF)-α, interleukin (IL)-12, reactive oxygen species (ROS), and reactive nitrogen species (RNS), which propagate aseptic inflammation, damage fibrous tissue, and eventually lead to implants rejection [17]. Consequently, it is

crucial to eliminate LPS along with sterilizing bacteria for refereeing immunomodulation and inhibiting pro-inflammatory and complications. In addition to inhibiting of M1 activation, an alternative way to promote the effect of PJI therapy is to enhance M2 activation, which is ascribed to the anti-inflammatory related cytokines releasing from M2, such as IL-4, IL13, IL-10, and transforming growth factor (TGF)-β [18]. These anti-inflammatory related cytokines are mostly involved with tissue repair.

Many methods are applied to polarize macrophages and endow materials superior bone repair ability. Surface structure is one of the key factors to regulate cell behavior. The roughness, modulus, morphologies and pore size were constructed on materials surface to polarize M0 to M2 subtype [19–21]. Chemical elements and surface functional groups were introduced for enhancing M2 activation. Bioactive molecule may excel them due to its multi-functions in nature [22,23]. Natural antimicrobial peptides (AMPs) is one of the bioactive molecule obtained in nature, which could be the best solution for the PJI due to their multiple functions [24–31]. AMPs, the short cationic and amphipathic host-defense molecules produced by constitutive or inducible expression in organs, play an important role in the host innate immunity and immunomodulatory functions. More than 4000 AMPs have been discovered to date according to the most recent antimicrobial peptides databases [32–34]. AMPs kill bacteria through saturating membrane, binding bacterial endotoxins (LPS) and neutralizing the biological effects of LPS. However, the high cytotoxicity, poor tissue distribution, susceptibility to proteolysis and hydrolysis, the development of allergies to the peptides, and the high cost involved in the synthesis of natural AMPs hamper their use as drug candidates. Peptidomimetics design is the first emergent choice to solve some of these problems due to its adjustable properties [35–39]. The mimetic AMPs can mimic the functions of natural AMPs, while avoiding enzymatic and hydrolysis degradation. To find a perfect peptidomimetic that can avoid various drawbacks of natural AMPs, many studies have been carried out, including the use of more cationic charges to decrease the cytotoxicity, the introduction of additional hydrophilic groups to finely mimic the biological activity of natural AMPs, the use of natural AMPs as template to mimic its immunomodulatory and so on. These peptidomimetics, unfortunately, are still high-cost and susceptible to proteolysis and hydrolysis *in vivo* environment. Therefore, it is of importance to find a new method to mimic the antibacterial and immunomodulatory mechanism of natural AMPs.

Puerarin is extracted form puerarin lobate, which can bind with LPS [40–45]. Chitosan is chosen as the bacteria puncture mimetic part due to its abundant cationic –NH₂ [6,46,47]. Consequently, in this work, a composite material via peptide free method that mimics the functions of AMPs was fabricated by solid reaction (Fig. 1). The immunomodulation ability of the samples was evaluated by subcutaneous air pouch model, and the osteogenesis properties of the samples was evaluated by rat

femoral osteomyelitis model. As the composite material is not peptide based molecule, it can escape the proteolysis and hydrolysis. An additional advantage of P@C is the low cost compared to peptidomimetics, as P@C is synthesized from cheap and available raw materials via simple fabrication route. In summary, the composite material presented in this work provides a novel and effective method for treating PJI in clinic.

2. Materials and methods

2.1. Materials

Chitosan (Aladdin) was dissolved in acetic acid and puerarin (Aladdin, 98%) was dissolved in 40% ethyl alcohol. The composite material (named P@C) was fabricated by solid reaction as following methods: 5 mg/mL chitosan was dissolved by adding 100 μL acetic acid, then 5.2 mg/mL puerarin was added into the dissolved chitosan. The composite material was fabricated through persistently grind until the solvent was almost evaporated to dry. Finally, P@C was dissolved by acetic acid. The methods of sulfonated PEEK and the drug loading process were expressed in Supplementary Materials.

2.2. In vitro antibacterial tests

2.2.1. Bacterial counting assay

Escherichia coli (*E. coli*, ATCC 25922, gram-negative bacterium), *Pseudomonas aeruginosa* (*P. aeruginosa*, ATCC 27853, gram-negative bacterium) and *Staphylococcus aureus* (*S. aureus*, ATCC 43300, a gram-positive bacterium) were used for detecting the antibacterial ability of samples. The bacterial counting assay was used to quantitatively calculate the antibacterial rate of samples. The bacteria were transferred onto the Luria-Bertani (LB) or tryptic soy broth (TSB) for another 16 h culture at 37 °C after culturing it on the samples surface for 24 h. The active bacteria were counted according to the National Standard of China GB/T 4789.2 protocol.

2.2.2. Bacterial morphology

Samples were cultured with 60 μL of the suspension at a bacteria concentration of 10⁷ CFU/mL at 37 °C for 24 h. At the specified incubation time, the samples were rinsed gently with PBS and fixed with 2.5% glutaraldehyde solution (Sigma-aldrich) overnight. The specimens were dehydrated in a series of ethanol solutions and dried in the series hexamethyldisilizane (HMDS) ethanol solution. The morphology of the bacteria was observed by SEM.

2.3. In vivo immune response in air pouch model

2.3.1. Subcutaneous implantation

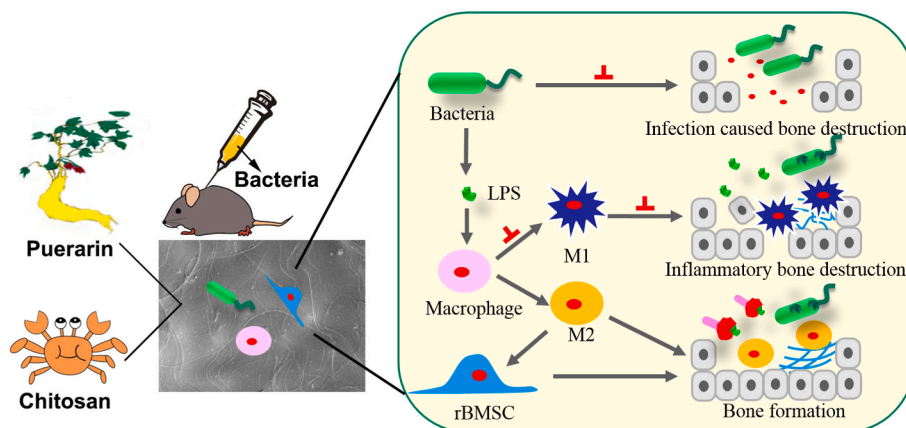The experimental protocol concerning animals used in this work was

Fig. 1. Schematic illustration of tissue repair after bacterial infection. When PJI occurs, bacteria would hurt cells and result in bone destruction. Chitosan, serving as the bacteria puncture agent, and puerarin, serving as the LPS target agent, synergistically and selectively destroy the negative bacterial membrane, which can inhibit the infection caused bone destruction. Only using antibacterial therapy, LPS induced inflammatory would cause bone destruction due to the inflammatory cytokines release form M1. Owing to the bond of puerarin ad LPS, macrophages tend to differentiate into M2 rather than M1, which can inhibit the inflammatory bone destruction. Besides, the composite material can promote rBMSCs differentiation, thus then accelerate bone formation.

approved by the Shanghai Tongren Hospital Ethics Committee (2021-090-01). 6 male C57BL/6 mice, 8 weeks old were used for each group. The skin was shaved and sterilized after anaesthetization with 4% chloral hydrate (16 mg/100 g). Then, the samples were inserted into the subcutaneous space and the incision was sutured and disinfected.

2.3.2. Histological analysis

The tissues of skin surrounding samples were harvested at 7 days post-surgery. After fixed and cut into 5 μm thickness sections, the tissue were stained with hematoxylin-eosin (H&E), Masson and immunohistochemistry. The procedures of immunofluorescence staining was put as follows: After blocked with 1% BSA for 30min, the tissue sections were incubated with primary antibody against CCR7 (1:50, ab52602, AbCam) and CD206 (1:50, ab64693, AbCam) at 4 °C overnight. Then, the tissue was incubated with goat anti-rat Alexa Fluor 488 (1:200, ab150165, AbCam), goat anti-rabbit Alexa Fluor 594 (1:200, ab150080, AbCam) secondary antibodies and DAPI. The samples were observed by fluorescent microscope (Leica, TCS SP8 SR). Image-Pro Plus software was used to quantitatively analyze the thickness of fibrous layer and the percentage of CCR7-positive (M1) or CD206-positive (M2) cells.

2.3.3. Theoretical calculation

Theoretical calculation of bond between LPS, TLR-4-MD2 and TLR-4-MD2-LPS and puerarin were calculated by AutoDock Tools. Firstly, the structure of LPS, TLR-4-MD2 and TLR-4-MD2-LPS were extracted from the structure of crystal structure of mouse TLR4/MD-2/LPS (PDB https://doi.org/10.2210/pdb3VQ2/pdb). The structure of puerarin was constructed by ChemDraw. Then, puerarin was inserted into the pocket of TLR4/MD-2, which was LPS in TLR4/MD-2/LPS. The interaction energies of the optimized structures were calculated by AutoDock Vina.

2.4. In vivo bone formation in osteomyelitis model

2.4.1. Rat femoral osteomyelitis model

The rat osteomyelitis model was used to evaluate the bone formation of samples under infection. 30 Sprague Dawley rats (3 months old, male) were separated to four groups, PEEK, SP, SPP, SPC, and SPP@C. The rats were anesthetized via intraperitoneal injection of 4% chloral hydrate (0.9 mL per 100 g rat weight), and the hind leg was shaved thoroughly and disinfected. Afterwards, the femoral condyle was exposed through making a medial patellar incision, and a hole axis of the femur was conducted to access the medullary cavity by drilling with a 2-mm diameter Kirschner wire. Subsequently, 10 μL of bacterial suspension at a concentration of 1×10^5 CFU/mL bacteria (*E. coli*) was injected into the drilled hole. The cylindrical sample (8 mm length and 2 mm diameter) was inserted into the drilled hole. Then, the skin and muscle were sutured and disinfected secondly. The rats were then housed in separate cages and free to eat and drink [48].

Alizarin red S (30 mg/kg), and calcein (20 mg/kg), were intraperitoneally injected into the rats at 4, and 6 weeks post-surgery, respectively, to detect the new bone formation surrounding the samples. After 8 weeks, the rats were sacrificed and the femurs with samples were harvested for further study.

2.4.2. Micro-CT analysis

The femurs with the samples were fixed for 2 days in 10% buffered formaldehyde. Then, micro-CT (SCANCO μCT50, Switzerland) was used to observe new bone formation. The samples were scanned at 70 kV and 357 μA using an Al 1-mm filter. Two-dimensional (2D) and three-dimensional (3D) models were reconstructed and generated using NRecon software (Skyscan, USA) and CTvol program (Skyscan). The percentage of new bone (bone volume/total volume, BV/TV) was calculated.

2.4.3. Histopathological evaluation

The femurs embedded with samples were dehydrated by graded

ethanol solutions and then embedded in poly (methyl methacrylate) (PMMA). The tissue was cut into 150-μm-thick sections and polished to final approximately 50 μm thickness. Hematoxylin & eosin staining (HE) and Van Gieson's picrofuchsin staining was performed to evaluate new bone formation surrounding the samples. Goldner staining and was applied to evaluate the mineralization bone. The maturity of newly formed bone was evaluated by Masson staining. Then, the newly formed bone surrounding the samples was observed using Intelligent digital slice scanning system (Hamamatsu NanoZoomer S60).

2.5. Data analysis

Quantitative data were analyzed using GraphPad Prism Version 7.0 statistical software (GraphPad Software, CA, USA) and were expressed as the mean ± standard deviation. Two-way analysis of variance and Tukey's multiple comparison tests were used to determine the significance of differences.

3. Results

3.1. Determination of P@C nanowire

The composite material was fabricated through solid-phase reaction and the scheme is shown in Fig. 2a. After reaction, P@C solution turns to milky from transparent. The light path in chitosan solution can be obviously observed, while there is not light path in puerarin solution, after reaction there is a light path in P@C solution, which indicates that P@C is homogeneous. To observe the morphology of P@C, the vacuum freeze was applied, and the results are showed in Fig. 2b. The diameter of P@C nanowires is 60–80 nm, and the length can be figured in the scale. To characterize the molecule structure of P@C, Fourier transform infrared spectroscopy (FTIR) was utilized to determine the reaction between chitosan and puerarin. As Fig. 2c shows, amide I (C=O), II (–NH$_2$), and III (C–N) band absorption peaks of chitosan appears at 1650 cm^{-1}, 1580 cm^{-1}, and 1336 cm^{-1} [49]. After reaction with puerarin, the amide II band moves to 1558 cm^{-1}, which denotes –NH$_2$ transfer to –NH– [50]. The stretching vibrations of phenolic hydroxyl groups at 1180–1260 cm^{-1} of puerarin weaken significantly after cross linking with chitosan, which indicates that the hydroxyl groups bond with other groups. The change of –NH$_2$ and weaker vibration of phenolic hydroxyl group after cross linking prove that chitosan chains cross links with each other through chemical bonds between amino group of chitosan and hydroxyl group of puerarin. To further determine the position of the hydroxyl of puerarin which combines with the amino group of chitosan, the carbon nuclear magnetic resonance (^{13}C NMR) was used, and the results are shown in Fig. 2d. Peak 1 comes from solvent. Peak 3 and 4 are the peaks that match the positions of the carbon marked in the puerarin molecule (position 3 and 4) in Fig. 2a. Whereas, peak 3 and 4 disappear after react with chitosan, which indicates that the hydroxyls connecting with the carbon 3 and 4 of puerarin combine with the amino of the chitosan. Besides, the peak 7 also disappears due to the change of the chemical environment of the adjacent carbon (position 7). Therefore, we deduce that the molecule structure of P@C as shown in Fig. 2a. The nano-wire was formed by self-assembly. The visible ultraviolet spectrophotometer (UV–Vis) was used to the determine the structure of the samples and results show that the characteristic peak at 300 cm^{-1} of P@C is the same as that of puerarin, indicating that the puerarin would not change its skeleton structure after combining with chitosan (Fig. 2e), which is consistent with the ^{13}C NMR results. As bone implants require superior mechanical properties, P@C is immobilized on the sulfonated PEEK surface through bonding with –SO$_3$H. After immobilization with P@C, the 3D network of sulfonated PEEK (denoted by SP) does not change (Fig. S1), which is verified to have favorable effects on cell adhesion, proliferation and osseointegration in our previous work [51].
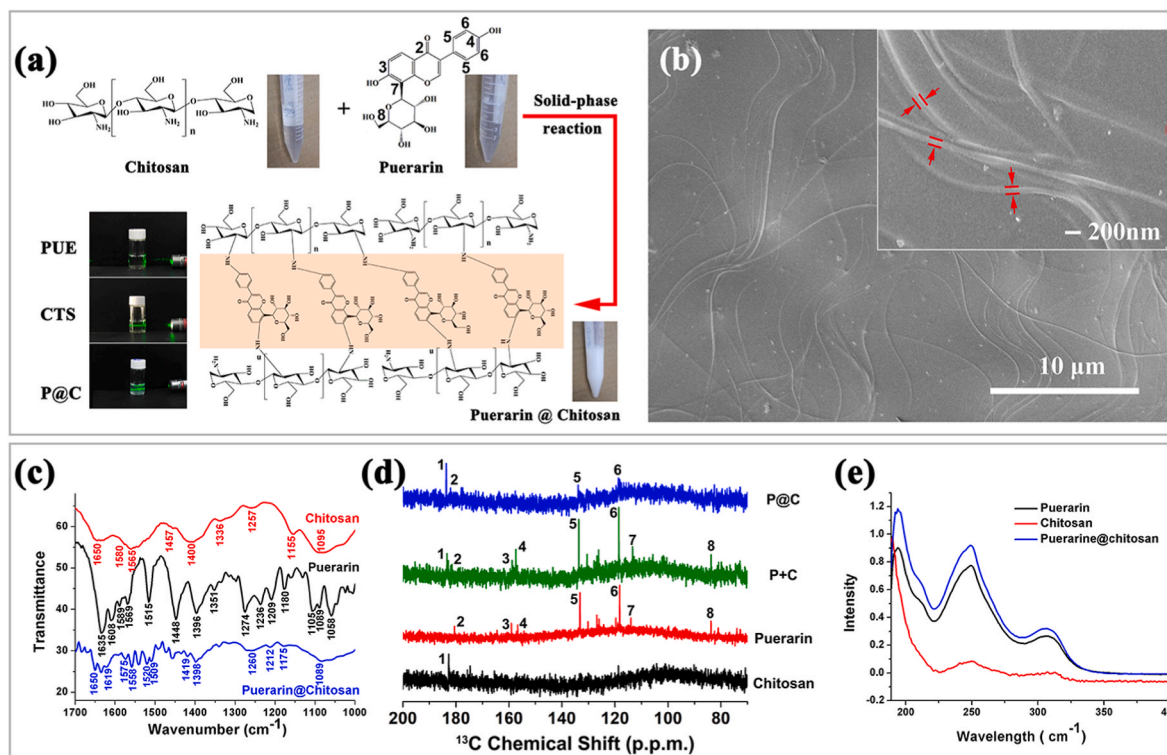
Fig. 2. Materials characterizations. Scheme of fabrication process and chemical formula of P@C: P@C is fabricated through solid-phase reaction, the –OH of puerarin bonds with the –NH$_2$ of chitosan, and the apparent solutions become milky after crosslinking (a, PUE: puerarin, CTS: chitosan). Morphology of P@C after lyophilization (b). FTIR of the samples (c). ^{13}C NMR analysis of samples. (e) UV–Vis of samples (d).

3.2. Antibacterial properties and LPS elimination properties

Escherichia coli (*E.coli*) was used to evaluate the antibacterial ability of the samples and the results are shown in Fig. 3a and **b**. The bacteria counting methods show that P@C has almost 100% antibacterial rate. Our previous work verified that the SP has good antibacterial ability against *E. coli* [51], however, the antibacterial ability of SP reduces after loading with puerarin due to the change of the chemical composition. Different from puerarin, chitosan kills bacteria through puncturing bacterial membrane. The bacteria, unfortunately, can recover their structure due to the fluid of the lipid bilayer, resulting in an unsatisfied antibacterial property (Fig. 3a, b, and d). By combining the functions of chitosan and puerarin, P@C can kill bacteria through puncturing cell membrane and bonding with LPS, synergistically destroying the structure of membrane fragments (Fig. 3a, b, and d and S2) and thus resulting in unrecoverable structure of the bacteria. To study the influence of P@C on bacteria membrane, TEM was applied and the results show that the integrated bacteria can be observed on the control group, while adding with P@C for 24 h, the hollow bacteria appears and the intensity of the membrane is ununiformed, which evidences that P@C possesses superior antibacterial ability against *E. coli* via puncture bacterial membrane (Fig. 3c). In addition to *E. coli*, P@C can effectively kill *Pseudomonas aeruginosa* (*P. aeruginosa*) due to its similar membrane structure to *E. coli* (Fig. S2). As shown in the SEM images (Fig. 3a), the membrane of most bacteria on SPP@C (the samples loading with P@C) is destroyed and the membrane of few bacteria on SPC (samples loading with chitosan) is destroyed, suggesting that the chitosan and P@C can kill bacteria through puncturing bacterial membrane. Based on this mechanism, we studied if the chitosan and puerarin through simple mixture possess same effect on bacteria (Fig. S3 and Fig. S4). After add the same puerarin content with P@C containing, the antibacterial ability is higher than chitosan, suggesting that the puerarin can enhanced the antibacterial ability of chitosan through LPS target. However, the antibacterial ability of simple mixing puerarin and chitosan is inferior compared to P@C,

which could be attributed to the better uniformity distribution of puerarin and chitosan in P@C that is favorable for synergistically puncturing bacteria membrane.

3.3. In vitro osteogenesis

The cell toxicity and differentiation evaluations show that P@C is more favorable for cell proliferation and differentiation than puerarin and chitosan (Fig. S5). P@C targets the specific molecule, LPS, which is the component of *E. coli* membrane rather than rBMSCs, so it selectively kills bacteria. The results of extracellular matrix (ECM) deposition shows that P@C is more favorable for ECM deposition at both 7 days and 14 days. However, compared to SP, SPP shows no obvious enhancement of ECM deposition at 7 days, and negligible enhancement at 14 days (Figs. S6 and 7).

3.4. In vivo immunomodulation

Vast LPS release often occurs along with excellent antibacterial ability, which would induce an over-activated immune response and leads to serious complications. Therefore, it is important to eliminate LPS along with sterilizing bacteria. LPS activates macrophages to differentiate into M1 subtype, which releases abundant inflammatory cytokines and lead to over-activated immune response. Here a subcutaneous air pouch model was used to evaluate the *in vivo* immune response of puerarin. The macrophages phenotype of collected tissue were evaluated by immunofluorescence stain. CCR7 labels M1 macrophages with red, CD206 labels M2 macrophages with green, and DAPI labels nuclei with blue. As Fig. 4a shows, the M1 active area is most, and green area is least among four groups. After loading puerarin onto SP, the green area is more. There are little red area and much green area in SPP@C group. Quantitative red and green fluorescence of samples normalized by blue fluorescence area are showed in Fig. 4b and **c** respectively. The ratio of M1 cells in PEEK group is most among four
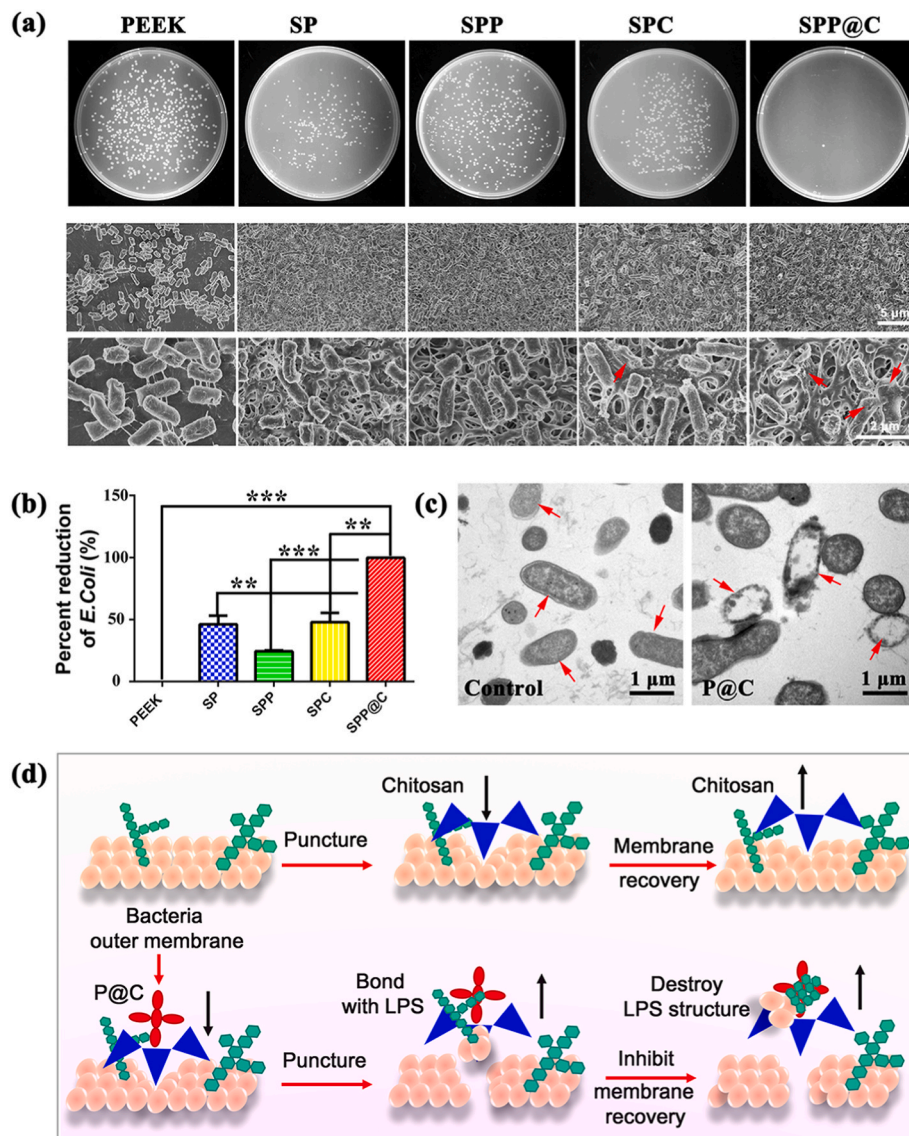
Fig. 3. *In vitro* bacteria responses. Photographs of the *E. coli* cultured for 24 h on samples and re-cultured on agars and morphologies of the *E. coli* after cultured for 24 h on samples (a). Quantitative results of antibacterial properties against *E. coli* based on bacteria counting methods (b). TEM images of the bacteria culture with or without P@C (c). Scheme of antibacterial mechanism: chitosan punctures bacterial membrane and thus kills bacteria. But the membrane of bacteria can recover its structure due to the fluid of lipid bilayer. P@C can puncture the bacterial membrane and bond with LPS, synergistically destroying the structure of the membrane fragments and thus exhibiting better antibacterial ability than chitosan. P@C can selectively puncture bacteria rather than cells due to its ability to target LPS, which is the specific component of bacterial membrane (d).

groups, and higher ratio of M2 cells occurs in SPP@C group.

The H&E and Masson staining of the tissue sections are shown in Fig. 5a. The fibrous tissue around PEEK is the thickest among these five groups, which indicates that the bad inflammatory occurs around PEEK. The thickness of fibrous tissue around SP is thinner than that around PEEK. After loading with puerarin and chitosan, the thickness of fibrous tissue further become thinner. The thickness of fibrous tissue around SPP@C is the thinnest among these five groups (Fig. 5b). In summary, P@C can activate macrophages into M2, and promote anti-inflammatory cytokine release, thus reducing the fibrous covering on the samples. LPS was recognized by TLR4-MD2 complex. To further explore the mechanism of C@P in immunomodulation, theoretical calculation was applied to predict the bond between molecules (Fig. 5c). Puerarin binds with LPS by physical bond due to their spatial conformation; their binding energy is −6.5 kcal/mol. Puerarin could insert into the pocket of TLR4-MD2. The bonding energy of this conjugation is −7.2 kcal/mol. Puerarin binds to TLR4-MD2-LPS by two hydrogen bonds with ARG337 and LYS360 in TLR4-MD2. The bonding energy of optimized conformation of puerarin and TLR4-MD2-LPS is −8.2 kcal/mol.

The mechanism of the effect of P@C on immune modulation is shown in Fig. 5d. LPS explosively releases once the bacteria are killed, then is recognized by toll like receptor 4, thus activating macrophages into M1

and causing inflammatory immune response, which is favorable for macrophage recruitment. On the one hand, P@C can bond with LPS, which can block the bioactive of LPS and result in M1 macrophage activation reduction. On the other hand, the released puerarin from P@C enhances the M2 macrophages activation. Therefore, the macrophages tend to differentiate into M2 rather than M1 in SPP@C group. As the H&E and Masson staining show, the fibrous tissue in SPP@C is slightly thicker than the samples loading with high puerarin content (SPP3), which is more favorable for tissue repair because the thin fibrous gives the hint of the bad blood vessel formation. The composite material (denoted by P@C) blocks the biological effects of LPS along with bacteria sterilization, which inhibits M1 activation. Furthermore, the composite material can promote M2 activation due to the natural immunomodulatory effect of puerarin part, which synergizes with the effect of M1 inhibition to promote tissue repair.

3.5. In vivo osteogenesis

Rat femoral osteomyelitis model was used to evaluate the *in vivo* antibacterial and osteogenic effect. The samples were inserted into the rat femur, which is injected with *E. coli*. After 8 weeks post-surgery, the rat femurs with the samples were collected for further evaluation. The
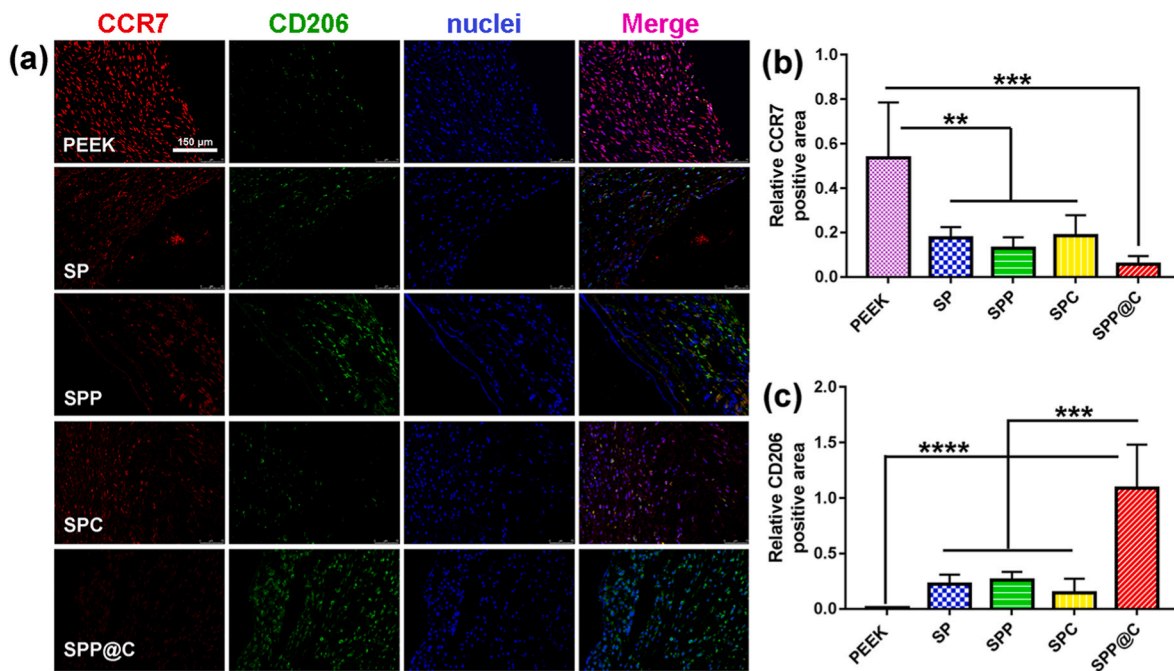
Fig. 4. Immune fluorescent images of the air pouch tissue around samples: the red fluorescence labels M1 marker, the green fluorescence labels M2 marker, and the blue fluorescence labels the nuclei of cells (a). Quantitative CCR7 positive area that normalized by nuclei (b). Quantitative CD206 positive area that normalized by nuclei (c).

micro-CT was used to evaluate the bone formation of the samples. The 2D micro-CT images show that the newly formed bone is tightly anchored on the samples, and the dynamic CT scan shows that the bone formation in SPP@C group is more than other groups. The reconstruction 3D micro-CT images visually show that the new bone formation in SPP@C is more than other samples. The quantitative results show that the order of bone volume/tissue volume area is: PEEK < SP < SPC < SPP < SPP@C (Fig. 6a, b and c). Fig. 6d shows the tissue slices investigated by fluorescent microscopy randomly. Around PEEK, only green fluorescence can be observed, which indicates that there is no early bone formation. Although the three colors of fluorescence can be observed in other groups, the gaps between fluorescent area and the surface of samples are obvious in SP and SPC. The quantitative results show that the order of fluorescence area is: PEEK < SP < SPC < SPP < SPP@C (Fig. 6e).

The rat femurs with the samples were incised into slice, and histopathological evaluation and the bone formation evaluation are shown in Fig. 7. H&E and Van Gieson's picrofuchsin staining were used to evaluate the newly formed bone around the samples under infection. Fig. 7a and b shows the images of HE staining with lower and higher magnification. There is more trabecula in SPP@C group than the other four groups. Images with higher magnification show that obvious bone destruction occurs in PEEK group, which are consistent with the Van Gieson's picrofuchsin staining results (Fig. 7c). Statistical results of new bone formation calculated from VG staining show that SPP@C can highly promote bone regeneration under infection due to its synergistic effect of superior antibacterial property and LPS elimination ability (Fig. 7d). While, SPP possesses LPS elimination effect and SPC possess antibacterial property but lack LPS eliminate effect. Therefore, the newly formed bone in SPP and SPPC is not satisfied. PEEK does not possess antibacterial property and immune modulation effect, exhibiting bacterial infection and bad bone destruction. Goldner staining was used to visualize the mineralized bone and the results are shown in Fig. 7e. The non-mineralized bone are stained with orange and mineralized bone are stained with green. As the images shown, obvious non-mineralized bone can be observed in PEEK, SP, and SPPC group, while there is little non-mineralized bone in SPC and SPP@C groups. The

statistical results show that the ratio of mineralized bone in PEEK groups is significantly lower than SPP@C (Fig. 7f). Masson staining was used to evaluate the bone maturation and the mature bone is labeled with red [52]. There are more mature bone in SPP@C compared with the other three groups (Fig. 7g). In summary, the mineralization and maturation of newly formed are related to the antibacterial ability of the samples.

4. Discussions

Bacterial infection is one of the main causes of failure bone repair. It is reported that 4%–10% nosocomial infections are caused by bacterial colonization [53]. Traditional bacteria treatment is constructing antibacterial coating surface. The strategies include anti-adhesion, contact killing and antibacterial agent release [54]. In this work, the antibacterial coating is designed based on the structure of bacteria. LPS is one of the main components of the negative bacterial membrane, and typically consists of lipid A, oligosaccharide, and O-antigen. It is a new idea to destroy bacteria structure through targeting LPS due to its important role in the interaction between bacterial cells [15]. Antimicrobial peptides are the natural biomolecules that can sterilize bacteria as well as inhibit inflammation through binding LPS and blocking the bio-functions of LPS. Therefore, searching a molecule to bind with LPS is essential for mimicking antimicrobial peptides. Chinese medicine is often to be chosen as the therapeutic agent for LPS induced inflammatory disease, such as puerarin, ginsenoside and Ginkgo biloba extraction [40,42,55–58]. In this work, puerarin is used to regulate immunomodulation of macrophage and chitosan were chosen to sterilize bacteria. Interestingly, a nanowire like hydrogel P@C was obtained, which also be verified in the previous work [59]. The amount of P@C nanowire increases with the puerarin content (Fig. S8). Notably, the antibacterial ability of the samples slightly increases with the puerarin content, which is attributed to the increased LPS bond ability of samples with higher puerarin content (Fig. S9, S10 and S11). However, the antibacterial ability of the samples with highest puerarin content is not yet satisfied. Puerarin can bond with LPS through matching their physical conformation, which inhibits communication of formation rather than punctures bacterial membrane. P@C can selectively puncture bacterial
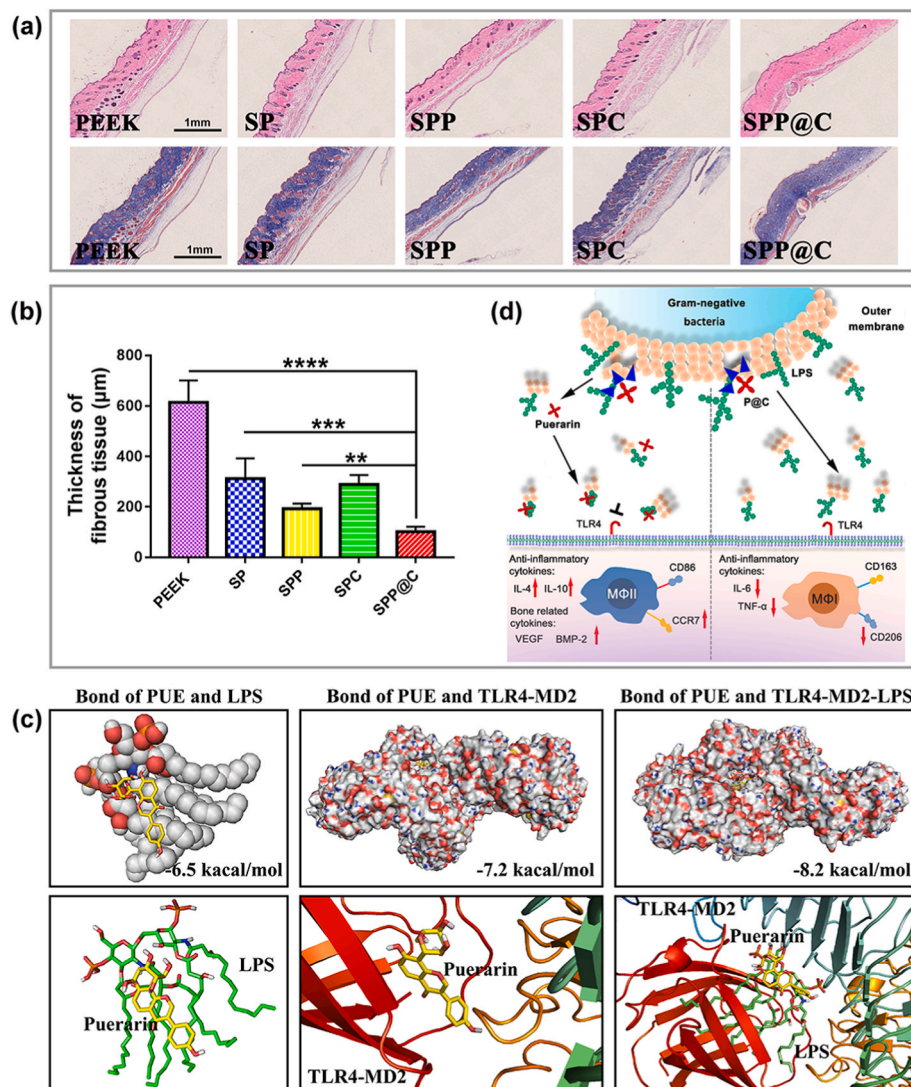
Fig. 5. In vivo immune response using subcutaneous air pouch model. H&E and Masson staining of tissue sections (a). Quantitative thickness of the fibrous tissue around the samples (b). Theoretical calculation of bond between LPS, TLR-4-MD2 and TLR-4-MD2-LPS and puerarin (c, PUE: puerarin). Scheme of immune response: chitosan cannot bond with LPS, which induces M1 activation. However, P@C and puerarin can bond with LPS and block its biofunction, thus promoting macrophages to differentiate into M2 rather than M1. Then M2 releases several anti-inflammatory cytokines, which are favorable for tissue repair (d).

membrane and inhibit its recovery through puncturing by chitosan and destroying the bacterial fragments by puerarin, thus synergistically sterilizing bacteria. The superior antibacterial properties of C@P than sole raw materials or simple mixture of them are attributed to two main factors: the first factor is the nanowire structure, which blocks the interaction of bacteria cells by entanglement, similarly to AMPs [60]; the second factor is the elevated zeta potentials, which adsorb bacteria to their surfaces and disturb charge balance by electrostatic interaction, resulting a better LPS target of PUE and a better membrane puncture of chitosan [61].

Even though treating with effective bacteria sterilization, an active immune that responds to LPS released from the lytic bacterial membrane always leading to failure osseointegration [62]. Macrophages are over activated by pathogen associated molecular patterns (PAMPs), which include LPS of Gram-negative bacteria, lipoteichoicacid (LTA) of Gram-positive bacteria, lipoarabinomannan (LAM) and peptidoglycan (PGN) of mycobacteria and so on. LPS releases along with the effective bacterial sterilization, which would immediately induce acute inflammatory responses through recognition by TLR4-MD2 heterodimer [63]. It should be noted that phosphate groups in lipid A is the active components to active pro-inflammatory response by myeloid differentiation primary response protein 88 (MyD88) mediated pro-inflammatory cytokines secretion [64]. However, similar structure to LPS paly inversed role in pro-inflammatory response. Eritoran, which has a closely

resembled structure to LPS, is endotoxin antagonist through competitively occupying the available space in TLR4-MD2 pocket [65]. This is one of the examples to prove that the small molecule, which could occupy the available space in TLR4-MD2 pocket, may be a useful inhibitor for the down-regulation of inflammation. Based on the theoretical calculation, puerarin could bind with TLR4-MD2 and TLR4-MD2/LPS, which inspired us that puerarin maybe the inhibitor in LPS induced inflammation. However, the details in bonds of puerarin and proteins and the mechanisms are worthy to be studied in the future researches. To determine the immunomodulation effect of puerarin, the samples with several contents of puerarin were subcutaneously implanted for further studies. H&E staining and Masson staining of the tissue sections show that the covering of fibrous tissue becomes thinner with the increasing puerarin content (Fig. S12), which is favorable for bone cell filtration. The fluorescence stains experiment shows that there are more M2 macrophages than M1 macrophages in all puerarin loaded samples (Fig. S13). Based on the above results, it can be concluded that puerarin can suppress M1 activation and promote M2 activation, and the effects are positively related with puerarin content. P@C can block the bioactive of LPS and promote M2 macrophage activation, which is related to the anti-inflammatory response and results in enhanced tissue repair.

The mechanism of pathogens damage tissue includes combination of exotoxin releasing from bacteria to induce apoptosis, endotoxin induced
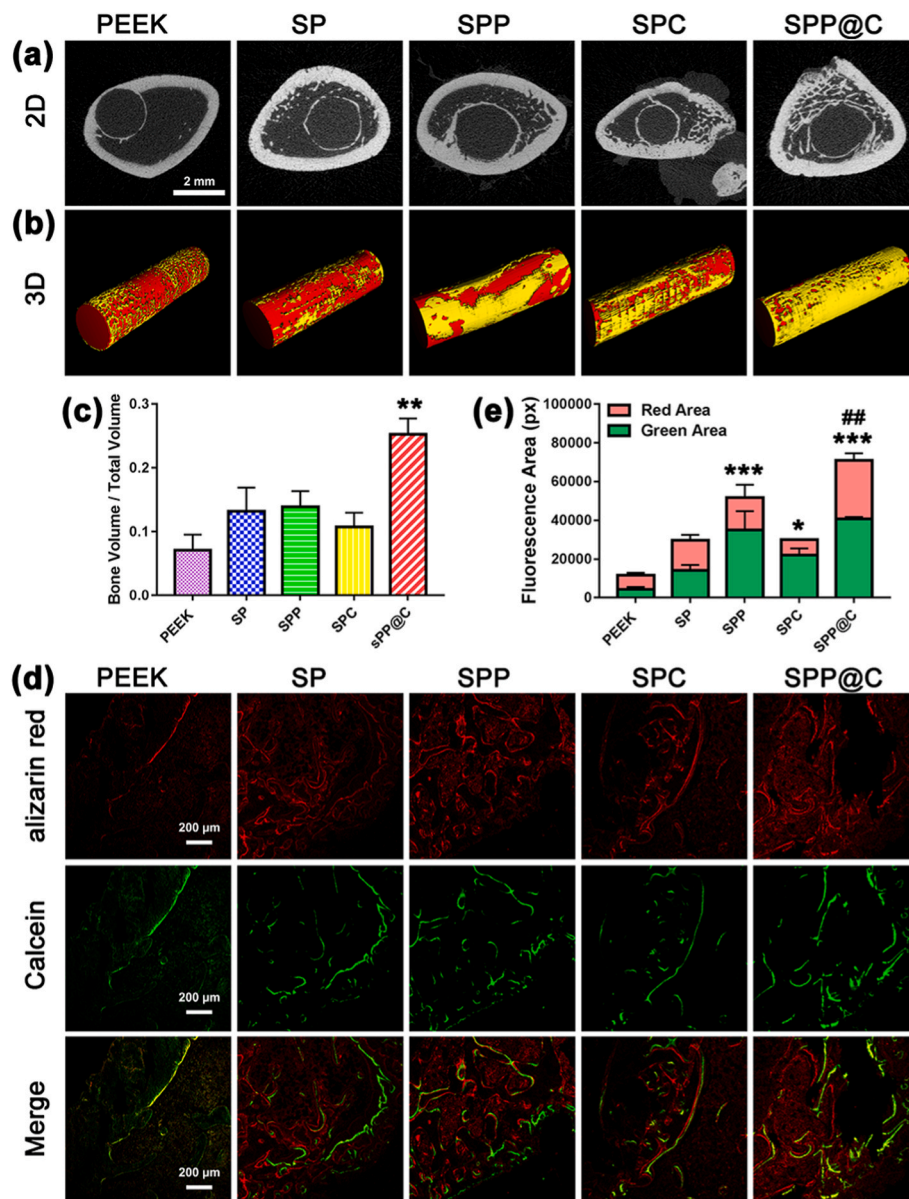
Fig. 6. 2D reconstruction micro-CT of samples (a) and 3D reconstruction micro-CT (b) of the samples. Quantitative bone volume/tissue volume of samples (c). Representative images of sequential fluorescence (e) and quantitative sequential Fluorescent Labeling of samples (d).

macrophage related immune response, and damage of intracellular bacteria. Based on these mechanisms, the elimination of pathogenic component is the same important as bacteria sterilization. It can be concluded from this work that the antibacterial coating designed based on targeting the pathogen component of bacteria is beneficial for both bacterial sterilization and immunomodulation. Except for LPS of Gram-negative bacteria, LTA of Gram-positive bacteria, LAM and PGN of mycobacteria are both the important component of maintaining bacterial structure and the PAMP of immune stimulant. Consequently, designing a material that could bind with LAM and PGN and block their bio-functions maybe new strategies for obtain implant surface with antibacterial and immunomodulatory effect.

5. Conclusions

In summary, the nanowire-like P@C was fabricated by combining chitosan and puerarin via solid-phase reaction. The as-prepared P@C can finely mimic the bio-functions of AMPs to destroy the bacterial membrane structure and inhibit its recovery by employing chitosan as

bacteria membrane puncture agent and puerarin as LPS target agent, thus exhibiting good antibacterial property. In addition, P@C possesses good osteoimmunomodulation owing to LPS elimination and macrophage differentiation modulation. The *in vivo* results show that P@C can inhibit the LPS induced bone destruction and sustaining fever post-surgery in the *E. coli* infected rat. P@C exhibits superior bone regeneration in *E. coli* infected rat due to the comprehensive functions of superior antibacterial ability, LPS elimination and immunomodulation. P@C can well mimic the functions of AMPs, providing a new method for the treatment of PJI in clinic.

Ethics approval and consent to participate

All animal experiments were approved and carried out with approval from the Shanghai Tongren Hospital Ethics Committee (2021-090-01).

CRediT authorship contribution statement

Liping Ouyang: Conceptualization, Data curation, Methodology,
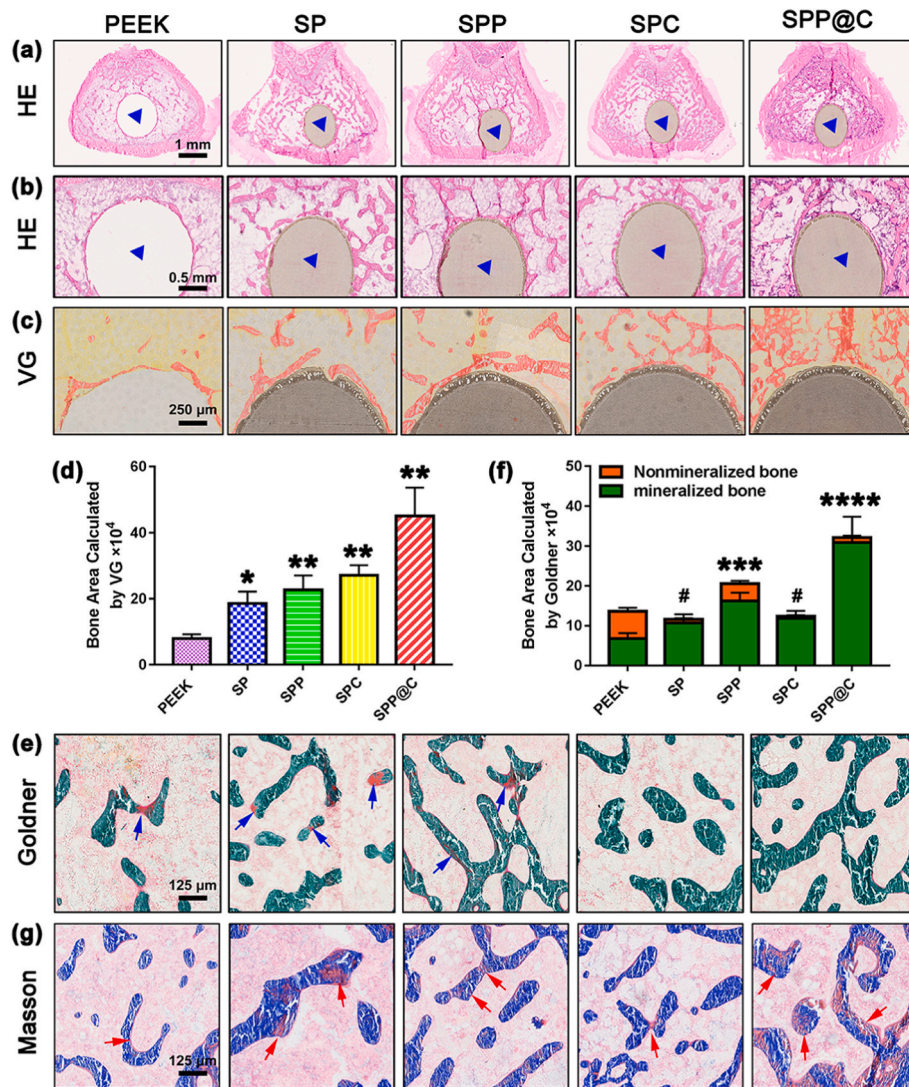
Fig. 7. Histopathological evaluation. (a) and (b) H&E staining of bone tissue implanted with samples post-surgery for 8 weeks. (c) Van Gieson's picrofuchsin staining of samples and corresponding statistical bone area (d). Representative images of Goldner staining (e, blue arrows marked the non-mineralization bone) and statistical results of mineralization bone and Non-mineralization bone (f). Representative images of Masson staining (g, green arrows marked the mature bone).

Formal analysis, Visualization, Data collection, Writing – original draft. **Baohui Chen:** Methodology, Data collection, Software. **Xingdan Liu:** Methodology, Data collection, Software. **Donghui Wang:** Writing – review & editing. **Yang Li:** Writing – review & editing. **Yun Liao:** Writing – review & editing. **Kelvin W.K. Yeung:** Writing – review & editing. **Xuanyong Liu:** Conceptualization, Funding acquisition, Project administration.

Declaration of competing interest

The authors declare that they have no known competing financial interests or personal relationships that could have appeared to influence the work reported in this paper.

Acknowledgements

Appendix A. Supplementary data

Supplementary data to this article can be found online at https://doi.org/10.1016/j.bioactmat.2022.09.005.

References

[1] C.A.M. Lowik, J. Parvizi, P.C. Jutte, W.P. Zijlstra, B.A.S. Knobben, C. Xu, K. Goswami, K.A. Belden, R. Sousa, A. Carvalho, J.C. Martinez-Pastor, A. Soriano, M. Wouthuyzen-Bakker, Debridement, antibiotics, and implant retention is a viable treatment option for early periprosthetic joint infection presenting more than 4 Weeks after index arthroplasty, Clin. Infect. Dis. 71 (2020) 630–636.
[2] H. Kapadia Bhaveen, A. Berg Richard, A. Daley Jacqueline, Fritz Jan, Bhave Anil, A. Mont Michael, Periprosthetic joint infection, Lancet 387 (2016) 386–394.
[3] R.O. Darouiche, Current concepts - treatment of infections associated with surgical implants, N. Engl. J. Med. 350 (2004) 1422–1429.
[4] W. Zimmerli, A. Trampuz, P.E. Ochsner, Current concepts: prosthetic-joint infections, N. Engl. J. Med. 351 (2004) 1645–1654.
[5] Y. Xia, X. Fan, H. Yang, L. Li, C. He, C. Cheng, R. Haag, ZnO/Nanocarbons-Modified fibrous scaffolds for stem cell-based osteogenic differentiation, Small (2020), e2003010.
[6] P. Li, Y.F. Poon, W. Li, H.Y. Zhu, S.H. Yeap, Y. Cao, X. Qi, C. Zhou, M. Lamrani, R. W. Beuerman, E.T. Kang, Y. Mu, C.M. Li, M.W. Chang, S.S. Leong, M.B. Chan-Park, A polycationic antimicrobial and biocompatible hydrogel with microbe membrane suctioning ability, Nat. Mater. 10 (2011) 149–156.

[7] N.G. Durmus, E.N. Taylor, K.M. Kummer, T.J. Webster, Enhanced efficacy of superparamagnetic iron oxide nanoparticles against antibiotic-resistant biofilms in the presence of metabolites, Adv. Mater. 25 (2013) 5706–5713.

[8] C. Yang, X. Ding, R.J. Ono, H. Lee, L.Y. Hsu, Y.W. Tong, J. Hedrick, Y.Y. Yang, Brush-like polycarbonates containing dopamine, cations, and PEG providing a broad-spectrum, antibacterial, and antifouling surface via one-step coating, Adv. Mater. 26 (2014) 7346–7351.

[9] J.S. Lee, W.L. Murphy, Functionalizing calcium phosphate biomaterials with antibacterial silver particles, Adv. Mater. 25 (2013) 1173–1179.

[10] A. Zarjou, L.M. Black, K.R. McCullough, T.D. Hull, S.K. Esman, R. Boddu, S. Varambally, D.S. Chandrashekar, W. Feng, P. Arosio, M. Poli, J. Balla, S. Bolisetty, Ferritin light chain confers protection against sepsis-induced inflammation and organ injury, Front. Immunol. 10 (2019) 1–15.

[11] A. Gordon, E.M. Greenfield, R. Eastell, E. Kiss-Toth, J.M. Wilkinson, Individual susceptibility to periprosthetic osteolysis is associated with altered patterns of innate immune gene expression in response to pro-inflammatory stimuli, J. Orthop. Res. 28 (2010) 1127–1135.

[12] Niebauer Josef, Volk Hans-Dieter, Michael Kemp, Dominguez Martin, R. Schumann Ralf, Rauchhaus Mathias, A. Poole-Wilson Philip, J.S. Coats Andrew, D. Anker Stefan, Endotoxin and immune activation in chronic heart failure: a prospective cohort study, Lancet 353 (1999) 1838–1842.

[13] D. Jo, D. Liu, S. Yao, R.D. Collins, J. Hawiger, Intracellular protein therapy with SOCS3 inhibits inflammation and apoptosis, Nat. Med. 11 (2005) 892–898.

[14] S.D. Wright, R.A. Ramos, P.S. Tobias, R.J. Ulevitch, J.C. Mathison, CD14, a receptor for complexes of lipopolysaccharide (LPS) and LPS binding-protein, Science 249 (1990) 1431–1433.

[15] C.R. Raetz, C. Whitfield, Lipopolysaccharide endotoxins, Annu. Rev. Biochem. 71 (2002) 635–700.

[16] O. Takeuchi, K. Hoshino, T. Kawai, H. Sanjo, H. Takada, T. Ogawa, K. Takeda, S. Akira, Differential roles of TLR2 and TLR4 in recognition of gram-negative and gram-positive bacterial cell wall components, Immunity 11 (1999) 443–451.

[17] Nemeth Krisztian, Leelahavanichkul Asada, S.T. Yuen Peter, Mayer Balazs, Parmelee Alissa, Doi Kent, G. Robey Pamela, Leelahavanichkul Kantima, H. Koller Beverly, M. Brown Jared, Hu Xuzhen, Jelinek Ivett, Star Robert A., Mezey Eva. Bone marrow stromal cells attenuate sepsis via prostaglandin E-2-dependent reprogramming of host macrophages to increase their interleukin-10 production, Nat. Med. 15 (2009) 42–49.

[18] R.D. Malefyt, J. Abrams, B. Bennett, C.G. Figdor, J.E. Devries, Interleukin-10 (IL-10) inhibits cytoines synthesis by human monocytes- an autoregulatory role of IL-10 produced by monocytes, J. Exp. Med. 174 (1991) 1209–1220.

[19] L. Chen, D. Wang, J. Qiu, X. Zhang, X. Liu, Y. Qiao, X. Liu, Synergistic effects of immunoregulation and osteoinduction of ds-block elements on titanium surface, Bioact. Mater. 6 (2021) 191–207.

[20] J. Lee, H. Byun, S.K. Madhurakkat Perikamana, S. Lee, H. Shin, Current advances in immunomodulatory biomaterials for bone regeneration, Adv Healthc Mater 8 (2019) e1801106.

[21] X. Zheng, L. Xin, Y. Luo, H. Yang, X. Ye, Z. Mao, S. Zhang, L. Ma, C. Gao, Near-infrared-triggered dynamic surface topography for sequential modulation of macrophage phenotypes, ACS Appl. Mater. Interfaces 11 (2019) 43689–43697.

[22] S.Y. Ji, H. Lee, H. Hwangbo, S.H. Hong, H.J. Cha, C. Park, D.H. Kim, G.Y. Kim, S. Kim, H.S. Kim, J.C. Yoo, Y.H. Choi, A novel peptide oligomer of bacitracin induces M1 macrophage polarization by facilitating Ca(2+) influx, Nutrients 12 (2020).

[23] Y. Zhang, J. Xu, Y.C. Ruan, M.K. Yu, M. O'Laughlin, H. Wise, D. Chen, L. Tian, D. Shi, J. Wang, S. Chen, J.Q. Feng, D.H. Chow, X. Xie, L. Zheng, L. Huang, S. Huang, K. Leung, N. Lu, L. Zhao, H. Li, D. Zhao, X. Guo, K. Chan, F. Witte, H. C. Chan, Y. Zheng, L. Qin, Implant-derived magnesium induces local neuronal production of CGRP to improve bone-fracture healing in rats, Nat. Med. 22 (2016) 1160–1169.

[24] M.E. Pachon-Ibanez, Y. Smani, J. Pachon, J. Sanchez-Cespedes, Perspectives for clinical use of engineered human host defense antimicrobial peptides, FEMS Microbiol. Rev. 41 (2017) 323–342.

[25] Lemaitre Bruno, Jules Hoffmann, The host defense of Drosophila melanogaster, Annu. Rev. Immunol. 25 (2007) 697–743.

[26] M.M. Cowan, Plant products as antimicrobial agents, Clin. Microbiol. Rev. 12 (1999) 564–582.

[27] M. Zasloff, Antimicrobial peptides of multicellular organisms, Nature 415 (2002) 389–395.

[28] E.W. Hancock Robert, Sahl Hans-Georg, Antimicrobial and host-defense peptides as new anti-infective therapeutic strategies, Nat. Biotechnol. 24 (2006) 1551–1557.

[29] T. Ganz, Defensins: antimicrobial peptides of innate immunity, Nat. Rev. Immunol. 3 (2003) 710–720.

[30] K.A. Brogden, Antimicrobial peptides: pore formers or metabolic inhibitors in bacteria? Nat. Rev. Microbiol. 3 (2005) 238–250.

[31] D.K. Dalton, S. Pittsmeek, S. Keshav, I.S. Figari, A. Bradley, T.A. Stewart, Multiple defects of immune cell- function in mice with disrupted interferon- gamma genes, Science 259 (1993) 1739–1742.

[32] Pirtskhalava Malak, Gabrielian Andrei, Phillip Cruz, L. Griggs Hannah, Squires R. Burke, E. Hurt Darrell, Grigolava maia, chubinidze mindia, gogoladze george, vishnepolsky boris, alekseev vsevolod, rosenthal alex, tartakovsky michael. DBAASP v.2: an enhanced database of structure and antimicrobial/cytotoxic activity of natural and synthetic peptides, Nucleic Acids Res. 44 (2016) D1104–D1112.

[33] Waghu Faiza Hanif, Barai Ram Shankar, Gurung Pratima, Idicula-Thomas Susan, CAMP(R3): a database on sequences, structures and signatures of antimicrobial peptides, Nucleic Acids Res. 44 (2016) D1094–D1097.

[34] Guangshun Wang, Li Xia, Zhe Wang, APD3: the antimicrobial peptide database as a tool for research and education, Nucleic Acids Res. 44 (2016) D1087–D1093.

[35] K. Hilpert, R. Volkmer-Engert, T. Walter, R.E. Hancock, High-throughput generation of small antibacterial peptides with improved activity, Nat. Biotechnol. 23 (2005) 1008–1012.

[36] E. Peisach, D. Casebier, S. Gallion, P. Furth, G. Petsko, J. Hogan, D. Ringe, Interaction of a peptidomimetic aminimide inhibitor with elastase, Science 269 (1995) 66–69.

[37] Rahmouni Sabri, Aaron Lindner, Rechenmacher Florian, Stefanie Neubauer, Sobahi Tariq Rashad Ali, Kessler Horst, Cavalcanti-Adam Elisabetta Ada, Spatz Joachim Pius, Hydrogel micropillars with integrin selective peptidomimetic functionalized nanopatterned tops: a new tool for the measurement of cell traction forces transmitted through alpha(v)beta(3) -or alpha(5)beta(1)-integrins, Adv. Mater. 25 (2013) 5869–5874.

[38] Nityakalyani Srinivas, Jetter Peter, J. Ueberbacher Bernhard, Werneburg Martina, Zerbe Katja, Steinmann Jessica, Van der Meijden Benjamin, Bernardini Francesca, Lederer Alexander, L.A. Dias Ricardo, E. Misson Pauline, Henze Heiko, Zumbrunn Juerg, O. Gombert Frank, Obrecht Daniel, Hunziker Peter, Schauer Stefan, Ziegler Urs, Kaech Andres, Eberl Leo, Riedel Kathrin, J. DeMarco Steven, John A. Robinson, Peptidomimetic antibiotics target outer-membrane biogenesis in Pseudomonas aeruginosa, Science 327 (2010) 1010–1013.

[39] J. Gabriel Gregory, Som Abhigyan, E. Madkour Ahmad, Tarik Eren, N. Tew Gregory, Infectious disease: connecting innate immunity to biocidal polymers, Mater. Sci. Eng. R Rep. 57 (2007) 28–64.

[40] Y. Zhang, M. Yan, Q.F. Yu, P.F. Yang, H.D. Zhang, Y.H. Sun, Z.F. Zhang, Y.F. Gao, Puerarin prevents LPS-induced osteoclast formation and bone loss via inhibition of akt activation, Biol. Pharm. Bull. 39 (2016) 2028–2035.

[41] Xiao Cheng, Li Jian, Xinxin Dong, Xiaojuan He, Xuyan Niu, Cha Liu, Guoyue Zhong, Rudolf Bauer, Dajian Yang, Aiping Lu, Anti-oxidative and TNF-α suppressive activities of puerarin derivative (4AC) in RAW264.7 cells and collagen-induced arthritic rats, Eur. J. Pharmacol. 666 (2011) 242–250.

[42] Yuan Yuan, Heng Zhou, Qing-Qing Wu, Li Fang-Fang, Zhou-Yan Bian, W.E.I. Deng, Zhou Meng-Qiao, Tang Qi-Zhu, Puerarin attenuates the inflammatory response and apoptosis in LPS-stimulated cardiomyocytes, Exp. Ther. Med. 11 (2016) 415–420.

[43] K. Singh Ashok, Yin Jiang, Shveta Gupta, Younus Mohamod, Ramzan Mohamod, Anti-inflammatory potency of nano-formulated puerarin and curcumin in rats subjected to the lipopolysaccharide-induced inflammation, J. Med. Food 16 (2013) 899–911.

[44] Y. Yuan, Q.Z. Tang, Puerarin reduces inflammatory responses and apoptosis in LPS-stimulated cardiomyoblasts, J. Am. Coll. Cardiol. 64 (2014) C49. C49.

[45] M.F. Melzig, R. Loose, Inhibition of lipopolysaccharide (LPS)-induced endothelial cytotoxicity by selected flavonoids, Planta Med. 64 (1998) 397–399.

[46] E.I. Rabea, M.E.T. Badawy, C.V. Stevens, G. Smagghe, W. Steurbaut, Chitosan as antimicrobial agent: applications and mode of action, Biomacromolecules 4 (2003) 1457–1465.

[47] S.K. Samal, M. Dash, S. Van Vlierberghe, D.L. Kaplan, E. Chiellini, C. van Blitterswijk, L. Moroni, P. Dubruel, Cationic polymers and their therapeutic potential, Chem. Soc. Rev. 41 (2012) 7147–7194.

[48] Xiangwei Yuan, Liping Ouyang, Luo Yao, Zhenjie Sun, Chao Yang, Jiaxing Wang, Xuanyong Liu, Xianlong Zhang, Multifunctional sulfonated polyetheretherketone coating with beta-defensin-14 for yielding durable and broad-spectrum antibacterial activity and osseointegration, Acta Biomater. 86 (2019) 323–337.

[49] J.G. Domszy, G.A.F. Roberts, Evaluation of infrared spectroscopic techniques for analyzing chitosan, Makromolekulare Chemie-Macromolecular Chemistry and Physics 186 (1985) 1671–1677.

[50] de Queiroz Antonino Rayane, Lia Fook Bianca, de Oliveira Lima Vítor, de Farias Rached Raid, Lima Eunice, da Silva Lima Rodrigo, Peniche Covas Carlos, Lia Fook Marcus, Preparation and characterization of chitosan obtained from shells of shrimp (Litopenaeus vannamei boone), Mar. Drugs 15 (2017) 141.

[51] Liping Ouyang, Yaochao Zhao, Guodong Jin, Tao Lu, Jinhua Li, Yuqin Qiao, Congqin Ning, Xianlong Zhang, K. Chu Paul, Xuanyong Liu, Influence of sulfur content on bone formation and antibacterial ability of sulfonated PEEK, Biomaterials 83 (2016) 115–126.

[52] Weijuan Huang, Cheng Shi, Xiaolan Wang, Yu Zhang, Lingyun Chen, Lina Zhang, Noncompressible hemostasis and bone regeneration induced by an absorbable bioadhesive self-healing hydrogel, Adv. Funct. Mater. 31 (2021), 2009189.

[53] A.Y. Peleg, D.C. Hooper, Hospital-acquired infections due to gram-negative bacteria, N. Engl. J. Med. 362 (2010) 1804–1813.

[54] M. Cloutier, D. Mantovani, F. Rosei, Antibacterial coatings: challenges, perspectives, and opportunities, Trends Biotechnol. 33 (2015) 637–652.

[55] Q. Huang, T. Wang, H.Y. Wang, Ginsenoside Rb2 enhances the anti-inflammatory effect of omega-3 fatty acid in LPS-stimulated RAW264.7 macrophages by upregulating GPR120 expression, Acta Pharmacol. Sin. 38 (2017) 192–200.

[56] D.T.N. Huynh, N. Baek, S. Sim, C.S. Myung, K.S. Heo, Minor ginsenoside Rg2 and Rh1 attenuates LPS-induced acute liver and kidney damages via downregulating activation of TLR4-STAT1 and inflammatory cytokine production in macrophages, Int. J. Mol. Sci. (2020) 21.

[57] B. Gargouri, J. Carstensen, H.S. Bhatia, M. Huell, G.P.H. Dietz, B.L. Fiebich, Anti-neuroinflammatory effects of Ginkgo biloba extract EGb761 in LPS-activated primary microglial cells, Phytomedicine 44 (2018) 45–55.

[58] Ilieva Iliyana, Ohgami Kazuhiro, Shiratori Kenji, Yoshikazu Koyama, Kazuhiko Yoshida, Kase Satoru, Kitamei Hirokuni, Takemoto Yuko, Yazawa Kazunaga, Shigeaki Ohno, The effects of Ginkgo biloba extract on lipopolysaccharide-induced inflammation in vitro and in vivo, Exp. Eye Res. 79 (2004) 181–187.

[59] S. Wang, B. Chen, L. Ouyang, D. Wang, J. Tan, Y. Qiao, S. Ge, J. Ruan, A. Zhuang, X. Liu, R. Jia, A novel stimuli-responsive injectable Antibacterial hydrogel to achieve synergetic photothermal/gene-targeted therapy towards uveal melanoma, Adv. Sci. 8 (2021), e2004721.

[60] M. Domingues Marco, M. Silva Patrícia, G. Franquelim Henri, A. Carvalho Filomena, A.R.B. Castanho Miguel, C. Santos Nuno, Antimicrobial protein rBPI21-induced surface changes on Gram-negative and Gram-positive bacteria, Nanomed. Nanotechnol. Biol. Med. 10 (2014) 543–551.

[61] B. Chen, H. Zhang, J. Qiu, S. Wang, L. Ouyang, Y. Qiao, X. Liu, Mechanical force induced self-assembly of Chinese herbal hydrogel with synergistic effects of antibacterial activity and immune regulation for wound healing, Small (2022), e2201766.

[62] H. Takayanagi, Inflammatory bone destruction and osteoimmunology, J. Periodontal. Res. 40 (2005) 287–293.

[63] U. Ohto, K. Fukase, K. Miyake, T. Shimizu, Structural basis of species-specific endotoxin sensing by innate immune receptor TLR4/MD-2, Proc. Natl. Acad. Sci. U. S. A. 109 (2012) 7421–7426.

[64] Z. Jiang, P. Georgel, X. Du, L. Shamel, S. Sovath, S. Mudd, M. Huber, C. Kalis, S. Keck, C. Galanos, M. Freudenberg, B. Beutler, CD14 is required for MyD88-independent LPS signaling, Nat. Immunol. 6 (2005) 565–570.

[65] H.M. Kim, B.S. Park, J.I. Kim, S.E. Kim, J. Lee, S.C. Oh, P. Enkhbayar, N. Matsushima, H. Lee, O.J. Yoo, J.O. Lee, Crystal structure of the TLR4-MD-2 complex with bound endotoxin antagonist Eritoran, Cell 130 (2007) 906–917.